

# Radial anisotropy in seismic reference models of the mantle

C. Beghein

Department of Earth, Planetary and Atmospheric Sciences, 77

Massachusetts avenue, Building 54-526, Cambridge, MA 02139, USA

J. Trampert

Department of Geosciences, Utrecht University, Budapestlaan 4, PO Box

80021, 3508 TA Utrecht, The Netherlands

H.J. van Heijst

Shell International Exploration and Production, Post Office Box 60, 2280

AB Rijkswijk, The Netherlands

---

C. Beghein, Department of Earth, Planetary, and Atmospheric Sciences, 77 Massachusetts avenue, Building 54-526, Cambridge, MA 02139, USA. (beghein@mit.edu)

J. Trampert, Department of Geosciences, Utrecht University, Budapestlaan 4, PO Box 80021, 3508 TA Utrecht, The Netherlands, (jeannot@geo.uu.nl)

H.J. van Heijst, Shell International Exploration and Production, Post Office Box 60, 2280 AB Rijkswijk, The Netherlands

**Abstract.** Sambridge's Neighbourhood Algorithm was applied to normal mode and surface wave phase velocity data to determine the likelihood of radial anisotropy in mantle reference models. This full model space search technique provides probability density functions for each model parameter, and therefore reliable estimates of resolution and uncertainty, without having to introduce unnecessary regularization on the model space. Our results for shear-wave anisotropy (described by parameter  $\xi$ ) show a fast decrease with depth with no significant deviation from PREM at any depth. The data do not require strong deviations from PREM for P-wave anisotropy either, except between 220 and 400 km depth and in the D'' layer. The intermediate parameter  $\eta$  might depart from PREM between 220 and 670 km depth. This implies a likely deeper P-wave anisotropy and  $\eta$ -anisotropy than S-wave anisotropy. The sign change in the anisotropic parameters across the 670-discontinuity found by other authors is not warranted by our data set, which is far more extensive than in previous studies. We found that density needs to be well resolved because we observe a high dependence of the results for P-wave related parameters on the presence or absence of density in the parameterization. S-wave anisotropy and  $\eta$  are less affected by density. A well-resolved negative density anomaly was found in the uppermost mantle, and a density excess was observed in the transition zone and the lowermost mantle which might be a seismic signature of the recently identified post-perovskite phase.

## 1. Introduction

It is now commonly accepted that the Earth's uppermost mantle is anisotropic. Laboratory experiments show that the most abundant minerals in the uppermost mantle possess high intrinsic anisotropy, and seismology reveals that anisotropy is present at these depths. This indicates the existence of an efficient mechanism capable of aligning uppermost mantle minerals over large scales. Seismological evidence for radial anisotropy at these depths was first inferred from the discrepancy between isotropic Love and Rayleigh wave phase velocity maps [Anderson, 1961]. This was confirmed by many other seismological studies. PREM [Dziewonski and Anderson, 1981] was the first reference model to incorporate radial anisotropy in the top 220 km of the mantle. Spherically averaged radial anisotropy was also found at larger depths by Montagner and Kennett [1996], in an attempt to reconcile body-wave and normal mode observations. They derived a new reference model that contained a small amount of radial anisotropy down to 1000 km depth and in the lowermost mantle. The rest of the lower mantle appears to be devoid of any seismic anisotropy, although both experimental [Chen et. al., 1998; Mainprice, 2000] and theoretical studies [Oganov et. al., 2001a; 2001b; Wentzcovitch et. al., 1998] demonstrate that lower mantle minerals are highly anisotropic. This can be explained in terms of superplastic flow [Karato, 1998], since deformation by diffusion creep does not result in any preferred orientation of minerals. Panning and Romanowicz [2004] recently derived a three-dimensional model of the whole mantle and found that the degree zero of their shear-wave anisotropy is dominant in the lowermost mantle, similar to what Montagner and Kennett [1996] found previously.

In this paper we decided to revisit the problem of the presence of anisotropy in reference mantle models because we believe that the trade-offs among the model parameters might have biased previous results. For example, *Panning and Romanowicz* [2004] imposed a proportionality factor between the different elastic parameters and density anomalies in order to invert only for the two shear-wave related parameters. In the case of *Montagner and Kennett* [1996], the authors inverted free oscillation data for attenuation, density and three of the five parameters characterizing radial anisotropy, using  $V_p$  and  $V_s$  from body wave models as constraints on the two other parameters in order to reconcile the two types of data. They included attenuation to reduce some of the discrepancy between the body wave models and the normal mode data. The remaining difference was explained by radial anisotropy down to 1000 km. While this might be an explanation for the observations, it can be argued that body waves preferentially sample fast regions [*Nolet and Moser*, 1993] introducing thus a fast bias into models which could lead to apparent attenuation and anisotropy in the Montagner and Kennett approach. Their final one-dimensional mantle models contained a few percents of anisotropy down to a depth of 1000 km, and they reported a possible change in the sign of the anisotropic parameters at the 670-discontinuity. *Karato* [1998] interpreted these sign changes as the signature of a horizontal flow above the discontinuity and a vertical flow in the top of the lower mantle. Clearly, the presence or absence of global radial anisotropy at large depths has large consequences for geodynamic and mineralogy, and it should be investigated more thoroughly.

The goal of the present research is to assess the robustness of this 1-D anisotropy and to determine whether it is constrained by the current normal mode and surface wave data.

We did not want to fix model parameters such as  $V_p$  or  $V_s$  because possible trade-offs with other parameters could affect the results for anisotropy. We did not include any prior information coming from body-waves, instead we used fundamental mode surface waves and overtones together with normal mode central frequencies. Because of the absence of body waves, we could safely neglect attenuation. The Neighbourhood Algorithm (NA) [Sambridge, 1999a; 1999b] was used to survey the parameter space and to find an ensemble of good data-fitting 1-D models of the mantle. This method provides posterior probability density functions (PPDFs) for each model parameter and returns valuable indications on their resolution and trade-offs. The PPDFs allow us to calculate the probability that anisotropy is required by the given data. Since the entire model space, including the model null-space, is sampled and since we do not perform an inversion, our results are not biased by the introduction of damping or any other unnecessary a priori information on the model space. Another advantage of this technique, compared to inversions, is that a much larger part of the valley of the cost function is explored, yielding reliable posterior model variances. While a classical inversion is much faster of course, it does not allow a reliable evaluation of uncertainty.

## 2. Data

Phase velocity maps can be expanded into spherical harmonics and their degree zero can be linearly related to perturbations in the one-dimensional structure of the Earth, similarly to normal mode central frequency shifts. The relation between Earth's structure and these data is given by *Dahlen and Tromp* [1998] :

$${}_k df = \int_0^a \delta \mathbf{m}(r)_k \mathbf{K}(r) r^2 dr \quad (1)$$

where  ${}_kdf$  represents normal mode central frequency shift measurements or the degree zero of a phase velocity map.  $k$  discriminates between different surface wave frequencies or different normal mode multiplets, and  $a$  is the radius of the Earth.  ${}_k\mathbf{K}(r)$  is the volumetric structure kernel for perturbation  $\delta\mathbf{m}(r)$  with respect to PREM [Dziewonski and Anderson, 1981].

The data we used included the degree zero of various surface wave phase velocity maps and central frequency shift measurements of mantle-sensitive normal modes obtained from the Reference Earth Model Website (<http://mahi.ucsd.edu/Gabi/rem.html>). Although core-sensitive modes would add important constraints on mantle structure and on the density near the core-mantle boundary, including them in the data set would force us to increase the number of model parameters. This is not feasible yet, due to the current computational limit of NA on a single processor. We thus took care not to include any core modes. The selected data constitute a large set of published and unpublished measurements for various types of motion (Rayleigh and Love waves, spheroidal and toroidal modes) for fundamental modes and for the first few overtone branches. Error estimates were also available with the measurements. We added eight fundamental mode Rayleigh and Love wave phase velocity models for periods between 40 and 275 seconds. At each selected period between 40 and 150 s, the models and assigned errors resulted from the averaged degree zero coefficient and its standard deviation calculated from different phase velocity maps [Trampert and Woodhouse, 1995; 1996; 2001; Ekström et. al., 1997; Laske and Masters, 1996; Wong, 1989; van Heijst and Woodhouse, 1999]. This should account for different measuring techniques of phase velocity, different data coverage and different regularization schemes in the construction of the maps at these periods. For periods larger

than 150 s, we used the models obtained by *Wong* [1989]. The obtained errors for Love and Rayleigh wave data decrease almost linearly between 40 and 100 seconds and the curves flatten between 100 and 150 seconds, similarly to the errors estimated by *Beghein et. al.* [2002] for degree two Rayleigh wave phase velocity maps. The model of *Wong* [1989] being the only one available to us at longer periods, we decided to assign a constant uncertainty to models with periods greater than 150 seconds. We assumed for convenience that the errors are Gaussian distributed, but there were far too few models to test this hypothesis. Finally, we added the degree zero of the overtone surface wave measurements made by *van Heijst and Woodhouse* [1999] for toroidal modes up to overtone number  $n = 2$  and spheroidal modes up to overtone number  $n = 5$ . Owing to the absence of corresponding variance estimates, we used the same error bars as those estimated for the fundamental mode surface wave phase velocity maps as a function of frequency. An analysis of the entire data set, error bars included, showed a good agreement between the data published on the Reference Earth Model Website, our averaged degree zero phase velocity data and the overtone measurements (see Fig. 1 for the fundamentals and the first overtone branche). The variations in path coverage of the different surfave wave mode branches do not affect the low spherical harmonic degrees of the phase velocity maps since spectral leakage was reduced when constructing the maps [e.g. *Trampert and Woodhouse*, 2001,2003].

In total, the data set employed was composed of 237 measurements for Rayleigh waves and spheroidal modes and 294 measurements for Love waves and toroidal modes. All data were corrected for the crustal model CRUST5.1 [*Mooney et. al.*, 1998].

### 3. Parameterization and method

An anisotropic medium with one symmetry axis is characterized by five independent elastic coefficients  $A$ ,  $C$ ,  $N$ ,  $L$  and  $F$ , in the notation of *Love* [1927]. Radial anisotropy occurs when the symmetry axis points in the radial direction. This type of anisotropy is usually described by three anisotropic parameters ( $\phi = 1 - C/A$ ,  $\xi = 1 - N/L$  and  $\eta = 1 - F/(A - 2L)$ ) and one P and one S velocity. Note that these definitions vary from author to author. The elastic coefficients are related to the wavespeed of P-waves travelling either vertically ( $V_{PV} = \sqrt{C/\rho}$ ) or horizontally ( $V_{PH} = \sqrt{A/\rho}$ ), and to the wavespeed of vertically or horizontally polarized S-waves ( $V_{SV} = \sqrt{L/\rho}$  or  $V_{SH} = \sqrt{N/\rho}$ , respectively). Parameter  $F$  is related to the speed of a wave travelling with an intermediate incidence angle. We parameterized the models with perturbations of these five elastic coefficients and perturbations of density with respect to PREM [*Dziewonski and Anderson*, 1981]. The corresponding sensitivity kernels are given in *Tanimoto* [1986], *Mochizuki* [1986] and *Dahlen and Tromp* [1998]. The relation between the data  ${}_k df$  and the perturbations in the structure of the Earth is then :

$$\begin{aligned}
 {}_k df = \int_{r_{cmb}}^a & [ {}_k K_A(r) dA(r) + {}_k K_C(r) dC(r) \\
 & + {}_k K_L(r) dL(r) + {}_k K_N(r) dN(r) \\
 & + {}_k K_F(r) dF(r) + {}_k K_\rho(r) d\rho(r) ] r^2 dr
 \end{aligned} \tag{2}$$

In this equation,  $r_{cmb}$  is the radius of the core-mantle boundary and  $a$  is the radius of the Earth. The mantle is radially divided in six layers. The bottom and top depths of these layers are, in kilometres, (2891, 2609), (2609, 1001), (1001, 670), (670, 400), (400, 220), (220, 24). This coarse parameterization is dictated by computational resources, not by the vertical resolution of the data. Although normal modes and phase velocity data

have a finite resolution, they have a much higher radial resolution than we are able to mode here. Consequently the results should be seen as an indication of the presence of anisotropy, rather than a detailed model. Conservation of the mass of the Earth and its moment of inertia were imposed following *Montagner and Kennett [1996]*. The NA is applied to equation 1 in order to obtain mantle models of radial anisotropy.

In the first stage of the NA, the model space is surveyed to identify the regions that best fit the data. A measure of the data fit must therefore be defined. We chose the  $\chi^2$  misfit which measures the average data misfit compared to the size of the error bar :

$$\chi^2 = \frac{1}{N} \sum_{i=1}^N \frac{({}_k d_{ob}^i - {}_k d_{pr}^i)}{{}_k \sigma^i} \quad (3)$$

where  $N$  is the total number of data,  ${}_k d_{ob}^i$  represents the  $i$ th observed data,  ${}_k d_{pr}^i$  is the  $i$ th predicted data and  ${}_k \sigma^i$  is the uncertainty associated with data  $i$ . The NA iteratively drives the search towards promising regions of the model space and simultaneously increases the sampling density in the vicinity of these good data-fitting areas. One of the characteristics of the NA, which makes it different from usual direct search approaches, is that it keeps information on all the models generated in the first stage, not only the good ones, to construct an approximate misfit distribution. This distribution of misfit is used as an approximation to the real PPDF and as input for the second stage of the NA, where an importance sampling of the distribution is performed. It generates a resampled ensemble which follows the approximate PPD and which is integrated numerically to determine the likelihood associated with each model parameter and the trade-offs. The reader is referred to *Sambridge [1999a, 1999b]* for more details about the method. The tuning of parameters is required to run each stage of the NA. The optimum values of these tuning parameters have to be found by trial and error as explained below. To broaden the survey as much

as possible, the two tuning parameters required for the first stage of the algorithm were kept equal. These two parameters are  $n_s$ , the total number of new models generated at each iteration, and  $n_r$ , the number of best data-fitting cells in which the new models are created (the model space is divided into Voronoi cells). Tuning parameters have also to be chosen to insure the convergence of the Bayesian integrals in the second stage.

The degree zero of the five elastic coefficients were perturbed up to 5 % of their amplitude in PREM. We purposefully do not address the non-linearity of the problem, but want to assess if the data require modest anisotropy which can be modelled by perturbation theory. This has the great advantage of linearizing our forward problem, and so far no indications of stronger anisotropy have been observed. Two sets of experiments were performed, one where no density variations were allowed and one where we searched for degree zero density anomalies up to 2 % in addition to perturbations in the five elastic coefficients.

#### 4. Results

In the first series of tests, we fixed the density anomalies  $d\rho$  to zero in each layer and in the second series of tests, we released the constraint on density and performed a model space search for perturbations of the five elastic coefficients that describe radial anisotropy and density. In this second case, we assumed that the layer situated between 1001 and 2609 km depth, which constitutes most of the lower mantle, is isotropic. This assumption is reasonable because we didn't observe any changes in this layer in the first set of runs, and it considerably eased our computational requirements.

We thus first studied a 30-dimension model space and a 33-dimension model space afterward. The limit of NA on a single processor is estimated to be approximately 24 parameters [*Sambridge, 1999b*], beyond which it becomes highly time-consuming. The

most reliable way to use the NA is by successively increasing the tuning parameters  $n_s$  and  $n_r$  (kept equal to broaden the search) in the first stage of NA, computing the likelihoods associated with each model parameter, and comparing the different results. Stability is achieved once the solution is independent of the way the model space was sampled. It is also a way to obtain all the models compatible with the data, without being trapped in a local minimum. Given our 'high dimensional problem', we could not afford to run NA with high tuning parameters within a reasonable amount of time. Instead, we performed several surveys with relatively small tuning parameters (by resampling between 5 and 20 best data-fitting cells at each iteration). By comparing the results of the different small size surveys, we could determine which parameters were well-constrained and which were not, according to the dependence of the results on the tuning parameters.

The individual distributions of  $\xi$ ,  $\phi$ ,  $\eta$  and  $d\rho/\rho$  obtained with  $n_s = n_r = 15$  are displayed in Fig. 2 to 5, and Table 1 gives some probability values for anisotropy in each layer, based on the integration of the normalized likelihoods. It should be noted that in PREM anisotropy is present only in the upper 220 km of the mantle (our top layer), and therefore  $d\xi = \xi$ ,  $d\phi = \phi$  and  $d\eta = \eta$  at any other depth. We can thus equivalently talk about the absolute value of the anisotropy or its perturbation in these other layers.

Fig. 2 represents the ensemble of models of shear-wave anisotropy (parameter  $\xi$ ) as a function of depth, and the color scale indicates the likelihood of anisotropy. In Table 1 we show the probability that  $d\xi = \xi - \xi_{prem}$  is positive, i.e. that  $|\xi| \geq |\xi_{prem}|$ . These results for S-wave anisotropy are mostly independent of the tuning parameters employed, only small changes occurred in  $dL$  and  $dN$  for the different trials. Our models show that no significant deviation from PREM in S-wave anisotropy is required by the data

at any depth, including the D'' layer. The probability of a departure from PREM is small in every layer, as shown in table 1. This contradicts the findings of *Montagner and Kennett* [1996] and *Panning and Romanowicz* [2004]. Our results are robust with respect to density anomalies (they did not strongly depend on the presence of  $d\rho$  in the model space) except in the lowermost mantle. The signal for  $d\xi$  was clearly negative in D'' when density anomalies were neglected but shifted towards zero when  $d\rho$  was explicitly inverted for (the changes occurred in the elastic parameter  $dN$  and not in  $dL$ ). In the first set of tests, where  $d\rho$  was zero, anisotropy was allowed in the bulk of the lower mantle (in the depth range 1001-2609 km), but no S-wave anisotropy was detected.

P-wave anisotropy was more affected than S-wave anisotropy by the introduction of density in the model space, indicating a higher dependence of P-wave related parameters on the presence of  $d\rho$  in the parameterization. Fig. 3 shows that the most likely  $\phi$  model, obtained including density variations in the parameterization, does not significantly deviate from PREM in the top layer (from 24 to 220 km depth) nor between 400 and 1000 km depth. However, there is a strong probability of a positive  $d\phi$  (and thus  $\phi$ ) between 220 and 400 km and a negative  $d\phi$  in the lowermost mantle (see Table 1), similar to the results of *Montagner and Kennett* [1996]. This means that we could expect about 1 % of P-wave anisotropy in these two layers, and that P-wave anisotropy extends deeper than S-wave anisotropy. The influence of the parameterization (including density anomalies or not) is highest in the two top mantle layers, where the sign of  $d\phi$  changed between the two series of tests. A similar behavior was observed for  $\phi$  in the transition zone. Fig. 3 does not display any change in  $\phi$  with respect to PREM in the depth range 400-670 km but, when no density variations were allowed we obtained a clear  $\phi > 0$ , which corresponds

to the results of *Montagner and Kennett* [1996], if their model is averaged over our layer parameterization. Similarly, our results do not show any significant P-wave anisotropy in the top of the lower mantle, but its presence is not completely unlikely, as shown in Table 1. Note also that  $\phi$  was more clearly positive at these depths when no density anomalies were included. In the experiment without density, we obtained a high probability (0.86) of  $\phi > 0$  between 1001 and 2609 km depth, but the amplitude was very small (around 0.5 %). Observing that the observed link between P-wave anisotropy and density tends to reduce the amplitude of anisotropy, the assumption of an isotropy mid mantle layer remains justified. The results for  $\phi$  in the lowermost mantle did not appear to be highly influenced by density. The amplitude of the most likely  $\phi$  was higher when no density anomalies were included, but the sign did not change.

The  $\eta$  models (Fig. 4) were generally not as highly affected by density as P-wave anisotropy. The most likely places where we could have  $d\eta > 0$  are between 220 and 400 km depth and in the transition zone. At other depths, NA produced  $\eta \simeq \eta_{prem}$ . The probability of departure from PREM is weak because the distributions are wide, but their peaks are close to 1 %, similar to model AK135-F of *Montagner and Kennett* [1996]. These two layers are also where the strongest dependence on the presence of density in the model space was detected. When we imposed  $d\rho = 0$ ,  $d\eta$  was clearly centred on zero at these depths. The introduction of density seems to push the signal towards slightly positive values, but the robustness of these perturbations in  $\eta$  is not easy to assess. Also, with  $d\rho = 0$ , we obtained a positive  $\eta$  between 1001 and 2609 km depth but the amplitude was so small that we believe the assumption  $d\eta = 0$  is valid.

The sensitivity tests of *Resovsky and Trampert* [2002] suggest that the data we employed can resolve the density variations with a degree of confidence. Given that density affects some of the results on anisotropy, we believe that the models including density are the most realistic. The models of density anomalies we obtained (Fig. 5 and Table 2) clearly show a density lower than in PREM in the top 220 km and an increase in density in the transition zone and in the lowermost mantle. At other depths, no significant departure from PREM is required by the data, but  $d\rho$  is not quite as well resolved in the depth ranges 220-400 km and 670-1000 km, as shown by the individual likelihoods. The negative perturbation in density in the uppermost mantle is inconsistent with *Montagner and Kennett* [1996], but the positive anomaly in the lowermost mantle is in agreement with their models, as well as with the recent study by *Masters and Gubbins* [2003]. The equivalent isotropic  $d\ln V_s$  and  $d\ln V_p$  were computed as well, but no strong deviations from PREM were required by the data, as the probability of positive  $d\ln V_s$  and  $d\ln V_p$  was close to 0.5 in all layers.

## 5. Discussion and conclusions

A direct search method was applied to normal mode central frequency shift measurements and to the degree zero of surface wave phase velocity maps to assess the likelihood of radial anisotropy and density anomalies in reference mantle models. Because both normal mode structure coefficients and phase velocity models result from the inversion of seismic spectrum, we should ideally apply the NA directly to the spectrum to retrieve Earth's structure, but current computational resources are not sufficient. We chose instead to analyze the non-uniqueness associated with the inversion of structure coefficients and phase velocity maps.

A high dependence of P-wave related parameters on the presence of density perturbations in the parameterization was found in most of the mantle, but S-wave or  $\eta$ -anisotropy were less affected its presence of density in the model space. We compared the spherically averaged models obtained here with independent 3D studies and found a good agreement in the upper mantle with models using fundamental mode data alone [*Beghein and Trampert, 2004a*] and overtone data [*Beghein and Trampert, 2004b*] alone. We did not find any significant deviation from PREM in shear-wave anisotropy anywhere in the mantle, which questions the results of *Montagner and Kennett [1996]*. Their models showed a few percents of anisotropy down to 1000 km depth, with a change of sign in parameter  $\xi$  across the 670-discontinuity, and possibly across the 410-discontinuity. Although their models are not totally incompatible with our range for  $\xi$ , they are far from our most likely solution. Looking at probabilities, we conclude that the changes of sign in  $\xi$  below and above the transition zone are not robustly constrained by the data. The observed dependence of  $\xi$  on density might be responsible for the anisotropy found by *Montagner and Kennett [1996]* or *Panning and Romanowicz [2004]* in the lowermost mantle. A finer parameterization would of course show more details, but because we find all models compatible with the data, the averages from our thick layers are representative of the finer details. Indeed, in *Beghein and Trampert [2004a]*, a finer parameterization of the uppermost mantle was employed and a positive degree zero  $d\xi$  was found in the upper 100 km and  $d\xi < 0$  between 100 and 220 km depth. This results in a decrease of S-wave anisotropy with depth within the uppermost mantle, with slightly less anisotropy than in PREM in the top 100 km and a little more anisotropy than in PREM below, as predicted

by *Montagner and Kennett* [1996]. Our results here simply average over these two layers and overall there is no perturbation.

At most depths we observed a strong dependence of P-wave related parameters on the presence of density anomalies in the parameterization. Departure from PREM in P-wave anisotropy is required by the data between 220 and 400 km depth, with  $d\phi > 0$ , and in the lowermost mantle, with  $d\phi < 0$ . This indicates deeper P-wave anisotropy than S-wave anisotropy. From a comparison with *Beghein and Trampert* [2004b], it appears that this feature is not constrained by the overtone data of *van Heijst and Woodhouse* [1999] but by the normal mode data.

The negative  $d\phi$  in the lowermost mantle was also found by *Montagner and Kennett* [1996], but it is the only signal of P-wave anisotropy compatible with ours. The change of sign in  $\phi$  observed by *Montagner and Kennett* [1996] across the 670-discontinuity is not confirmed by our data.

Parameter  $\eta$  did not deviate strongly from PREM, except maybe between 220 and 670 km depth, where the probability of  $d\eta > 0$  is close to 0.7 (Table 1). This might indicate that  $\eta$ -anisotropy goes deeper than P-wave or S-wave anisotropy, but this is not supported by the overtone data alone [*Beghein and Trampert*, 2004b]. We did not find any clear sign of  $\eta$ -anisotropy in the lowermost mantle, but the uncertainty is very large.

It was clearly demonstrated that classical inversions of normal mode and surface wave data cannot find reliable variations in density due to a small sensitivity to the data [*Resovsky and Ritzwoller*, 1999; *Resovsky and Trampert*, 2002; *Romanowicz*, 2001]. In addition, damped inversions always underestimate model amplitudes, the more so if the sensitivity is small. In such cases, the NA is the best tool to put robust bounds on density

anomalies inside the Earth. *Resovsky and Trampert* [2002] showed that our data set could resolve density variations using NA. The density models we obtained were very different from those derived by *Montagner and Kennett* [1996]. This, added to the influence density anomalies has on the other parameters, resulted in differences in the models of anisotropy. We obtained a clear deficit in density in the uppermost mantle, and an excess of density in the transition zone and the lowermost mantle. This increase inside D” could be the signature of the recently observed post-perovskite phase [*Murakami et. al.*, 2004; *Oganov and Ono*, 2004; *Tsuchiya et al.*, 2004; *Shieh et. al.*, 2004].

**Acknowledgments.** We thank Malcolm Sambridge for sharing his Neighbourhood Algorithm, and Gabi Laske and Guy Masters for maintaining the Reference Earth Model (REM) website and making a large long-period seismic database available. We are grateful to Jeremy W. Boyce for his help while making the figures displayed in this article. Jeroen Ritsema and an anonymous reviewer gave helpful comments on the manuscript.

## References

- Anderson, D. L. (1961), Elastic wave propagation in layered anisotropic media, *J. Geophys. Res.*, *66*, pp. 2953–2963.
- Beghein, C., Resovsky, J., and Trampert, J. (2002), P and S tomography using normal mode and surface wave data with a neighbourhood algorithm, *Geophys. J. Int.*, *149*, pp. 646–658.
- Beghein, C., and Trampert, J. (2004a), Probability density functions for radial anisotropy from fundamental mode surface wave data and the Neighbourhood Algorithm, *Geophys. J. Int.*, *157*, pp. 1163–1174.

- Beghein, C., and Trampert, J. (2004b), Probability density functions for radial anisotropy: implications for the upper 1200 km of the mantle, *Earth Planet. Sci. Lett.*, *217*, pp. 151–162.
- Chen, G., Liebermann, R. C., and Weidner, D. J. (1998), Elasticity of single-crystal MgO to 8 Gigapascals and 1600 Kelvin, *Science*, *280*, pp. 1913–1915.
- Dahlen, F.A., and Tromp, J. (1998), *Theoretical Global Seismology*, Princeton Univ. Press, Princeton, New Jersey.
- Dziewonski, A., and Anderson, D. L. (1981), Preliminary reference Earth model, *Phys. Earth Planet. Inter.*, *25*, pp. 25297–25356.
- Ekström, G., Tromp, J., and Larson, E. W. F. (1997), Measurements and global models of surface wave propagation, *J. Geophys. Res.*, *102*, pp. 8137–8157.
- Mooney, W., Laske, G., and Masters, G. (1998), Crust 5.1 : a global crustal model at 5 deg  $\times$  5 deg, *J. Geophys. Res.*, *132*, pp. 727–747.
- Karato, S. (1998), Seismic anisotropy in the deep mantle, boundary layers and the geometry of mantle convection, *Pure Appl. Geophys.*, *151*, pp. 565–587.
- Laske, G., and Masters, G. (1996), Constraints on global phase velocity maps from long-period polarization data, *J. Geophys. Res.*, *101*, pp. 16059–16075.
- Love, A.E.H. (1927), *A Treatise on the Theory of Elasticity*, Cambridge Univ. Press.
- Mainprice, D., Barruol, G., and Ismail, W. B. (2000), The seismic anisotropy of the Earth’s mantle : from single crystal to polycrystal, in *Earth’s Deep Interior: Mineral Physics and Tomography From the Atomic to the Global Scale, Seismology and Mineral Physics, Geophys. Monogr. Ser.*, vol. 117, edited by S. Karato, pp. 237–264, AGU, Washington, D.C.

- Masters, G., and Gubbins, D. (2003), On the resolution of density within the Earth, *Phys. Earth Planet. Inter.*, *140*, pp. 159–167.
- Mochizuki, E. (1986), The free oscillations of an anisotropic and heterogeneous Earth, *Geophys. J. R. astr. Soc.*, *86*, pp. 167–176.
- Montagner, J.-P., and Kennett, B. L. N. (1996), How to reconcile body-wave and normal-mode reference Earth models, *Geophys. J. Int.*, *125*, pp. 229–248.
- Murakami, M., Hirose, K., Kawamura, K., Sata, N., and Ohishi, Y. (2004), Post-Perovskite Phase Transition in  $MgSiO_3$ , *Science*, *304*, pp. 855–858.
- Nolet, G., and Moser, T. J. (1993), Teleseismic delay times in a 3-D Earth and a new look at the S-discrepancy, *Geophys. J. Int.*, *114*, pp. 185–195.
- Oganov, A. R., Brodholt, J. P., and Price, D. (2001a), The elastic constants of  $MgSiO_3$  perovskite at pressures and temperatures of the Earth’s mantle, *Nature*, *411*, pp. 934–937.
- Oganov, A. R., Brodholt, J. P., and Price, D. (2001b), Ab initio elasticity and thermal equation of state of  $MgSiO_3$  perovskite, *Earth Planet. Sci. Lett.*, *184*, pp. 555–560.
- Oganov, A. R., and Ono, S. (2004), Theoretical and experimental evidence for a post-perovskite phase of  $MgSiO_3$  in Earth’s D’ layer, *Nature*, *430*, pp. 445–448.
- Panning, M., and Romanowicz, B. (2004), Inferences on flow at the base of Earth’s mantle based on seismic anisotropy, *Science*, *303*, pp. 351–353.
- Resovsky, J., and Ritzwoller, M. (1999), Regularization uncertainty in density models estimated from normal mode data, *J. Geophys. Res.*, *26*, pp. 2319–2322.
- Resovsky, J., and Trampert, J. (2002), Reliable mantle density error bars : An application of the Neighbourhood Algorithm to normal mode and surface wave data, *Geophys. J.*

*Int.*, 150, pp. 665–672.

- Romanowicz, B. (2001), Can we resolve 3D heterogeneity in the lower mantle?, *Geophys. Res. Lett.*, 28, pp. 1107–1110.
- Sambridge, M. (1999a), Geophysical inversion with a neighbourhood algorithm-I. Searching a parameter space, *Geophys. J. Int.*, 138, pp. 479–494.
- Sambridge, M. (1999b), Geophysical inversion with a neighbourhood algorithm-II. Appraising the ensemble, *Geophys. J. Int.*, 138, pp. 727–746.
- Shieh, S. R., Duffy, T. S., and Shen, G. (2004), Elasticity and strength of calcium silicate perovskite at lower mantle pressure, 143-144, pp. 93–105.
- Tanimoto, T. (1986), Free oscillations of a slightly anisotropic Earth, *Geophys. J. R. astr. Soc.*, 87, pp. 493–517.
- Trampert, J., and Woodhouse, J. H. (1995), Global phase velocity maps of Love and Rayleigh waves between 40 and 150 seconds, *Geophys. J. Int.*, 122, pp. 675–690.
- Trampert, J., and Woodhouse, J. H. (1996), High resolution global phase velocity distributions, *Geophys. Res. Lett.*, 23, pp. 21–24.
- Trampert, J., and Woodhouse, J. H. (2001), Assessment of global phase velocity models, *Geophys. J. Int.*, 144, pp. 165–174.
- Trampert, J., and Woodhouse, J. H. (2003), Global anisotropic phase velocity maps for fundamental mode surface waves between 40 and 150 s, *Geophys. J. Int.*, 154, pp. 154–165.
- Tsuchiya, T., Tsuchiya, J., Umemoto, K., and Wentzcovitch, R. M. (2004), Phase transition in  $MgSi_3$  perovskite in the earth’s lower mantle, *Earth Planet. Sci. Lett.*, 224, pp. 241–248.

Wentzovitch, R. M., Karki, B., Karato, S., and Da Silva, C. R. S. (1998), High pressure elastic anisotropy of  $MgSiO_3$  perovskite and geophysical implications, *Earth Planet. Sci. Lett.*, 164, pp. 371–378.

Wong, Y.K. (1989), *Upper mantle heterogeneity from phase and amplitude data of mantle waves*, PhD thesis, Cambridge, MA.

**Figure 1.** Ensemble of data and estimated errors for the fundamental surface wave and normal mode data (left) and for the first overtone branche (right) at different periods. Note the logarithmic scale on the horizontal axis.

**Figure 2.** Ensemble of shear-wave anisotropy models compatible with the data. The color scale represents the normalized likelihood associated with anisotropy in each layer. The individual marginals were normalized to 1, so that the  $1/e$  (orange) and  $1/e^2$  (yellow) contours correspond to 1 and 2 standard deviation, respectively. Darker colors correspond to more likely values of the parameter. The vertical blue line represents the value of  $\xi$  in model PREM, averaged over our layer parameterization.

**Figure 3.** Ensemble of P-wave anisotropy models compatible with the data. See caption of Fig. 2 for details. The vertical blue line represents the value of  $\phi$  in model PREM, averaged over our layer parameterization.

**Figure 4.** Ensemble of models for parameter  $\eta$  compatible with the data. See caption of Fig. 2 for details. The vertical blue line represents the value of  $\eta$  in PREM, averaged over our layer parameterization.

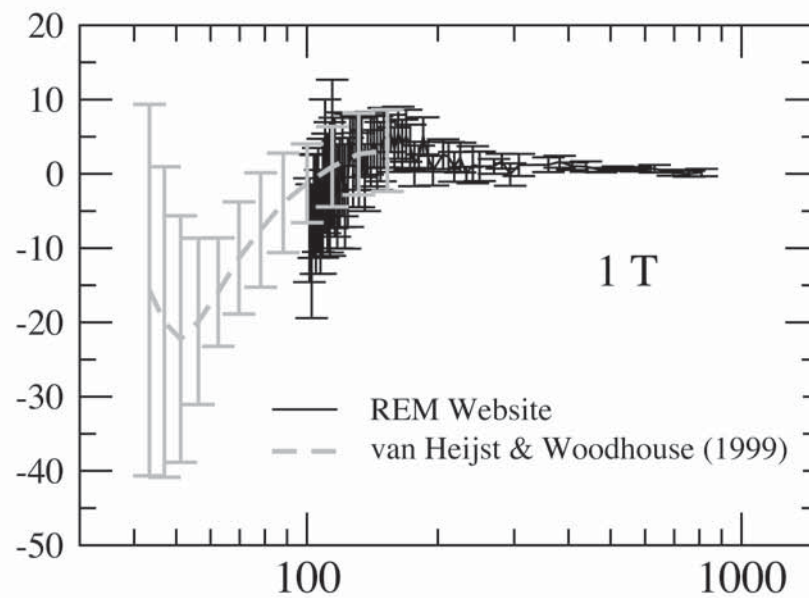
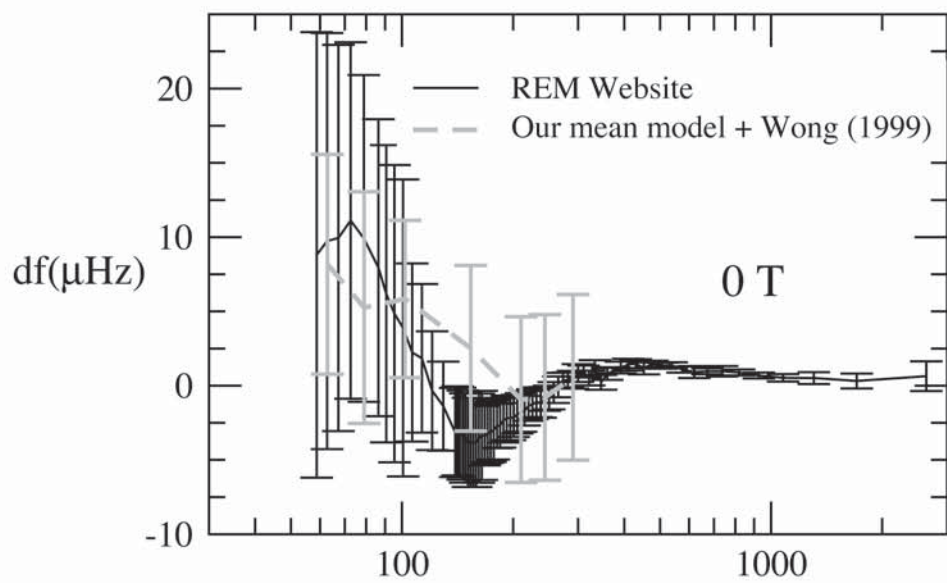
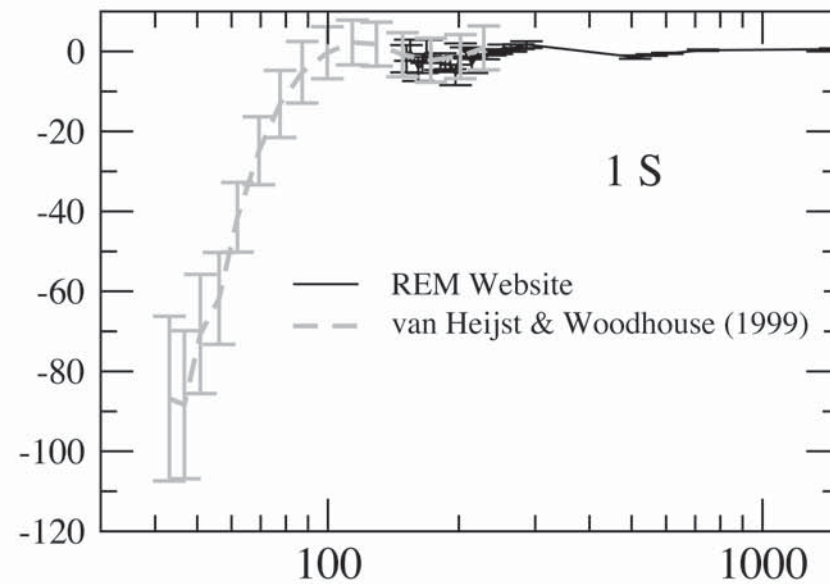
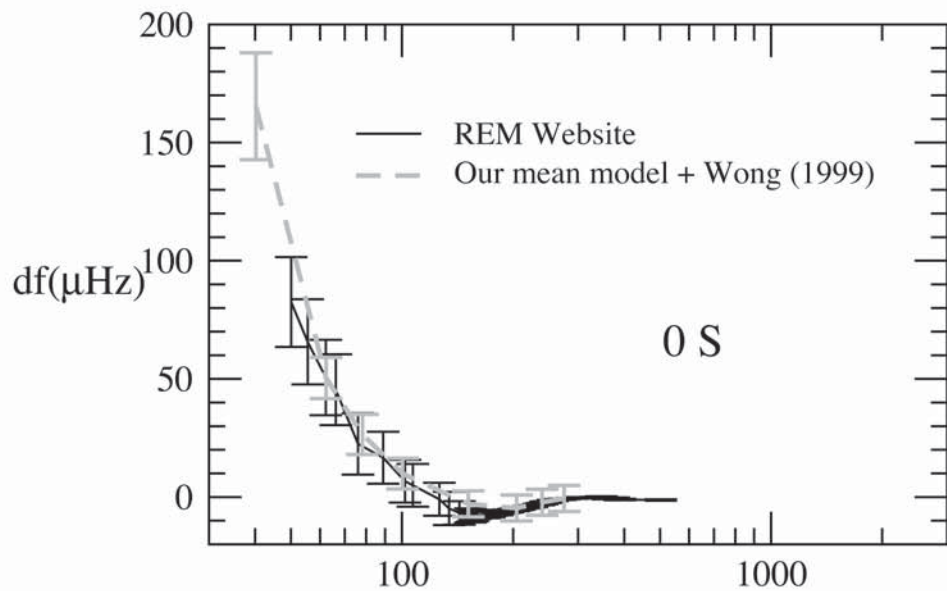
**Figure 5.** Ensemble of models of density anomalies that can explain the data. The full range of models is shown. Perturbations are with respect to PREM. See caption of Fig. 2 for details.

**Table 1.** Probability of having positive perturbations in anisotropic parameter  $p$ 

Parameter $p$	Depth (km)	$P(dp > 0)$
$\xi = 1 - N/L$	$24 < d < 220$	0.44
	$220 < d < 400$	0.47
	$400 < d < 670$	0.36
	$670 < d < 1001$	0.41
	$2609 < d < 2891$	0.35
$\phi = 1 - C/A$	$24 < d < 220$	0.42
	$220 < d < 400$	0.80
	$400 < d < 670$	0.49
	$670 < d < 1001$	0.62
	$2609 < d < 2891$	0.26
$\eta = 1 - F/(A - 2L)$	$24 < d < 220$	0.39
	$220 < d < 400$	0.68
	$400 < d < 670$	0.69
	$670 < d < 1001$	0.44
	$2609 < d < 2891$	0.43

**Table 2.** Probability of having positive density anomalies

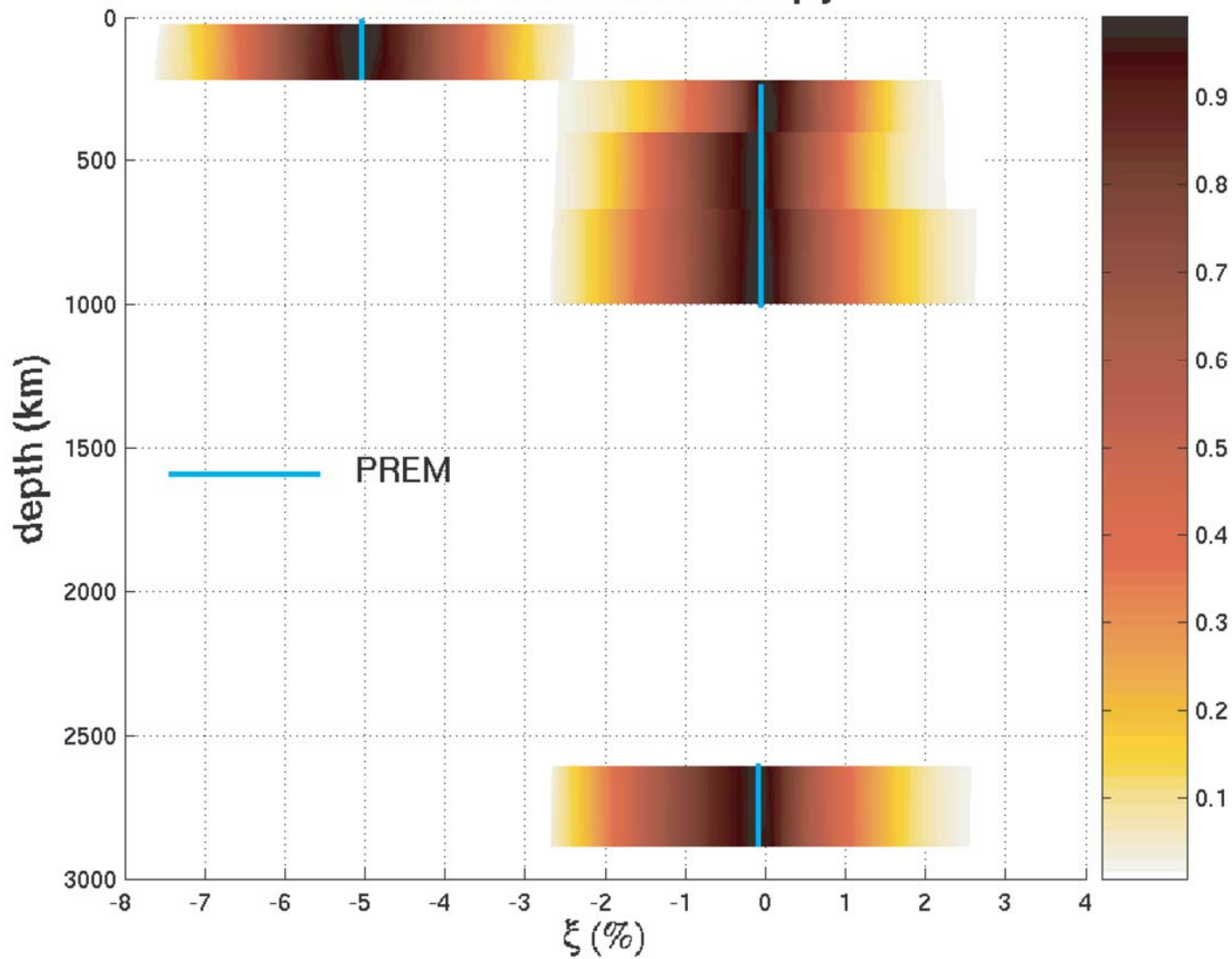
Depth (km)	$P(d\rho/\rho > 0)$
$24 < d < 220$	0.28
$220 < d < 400$	0.50
$400 < d < 670$	0.71
$670 < d < 1001$	0.57
$1001 < d < 2609$	0.40
$2609 < d < 2891$	0.72



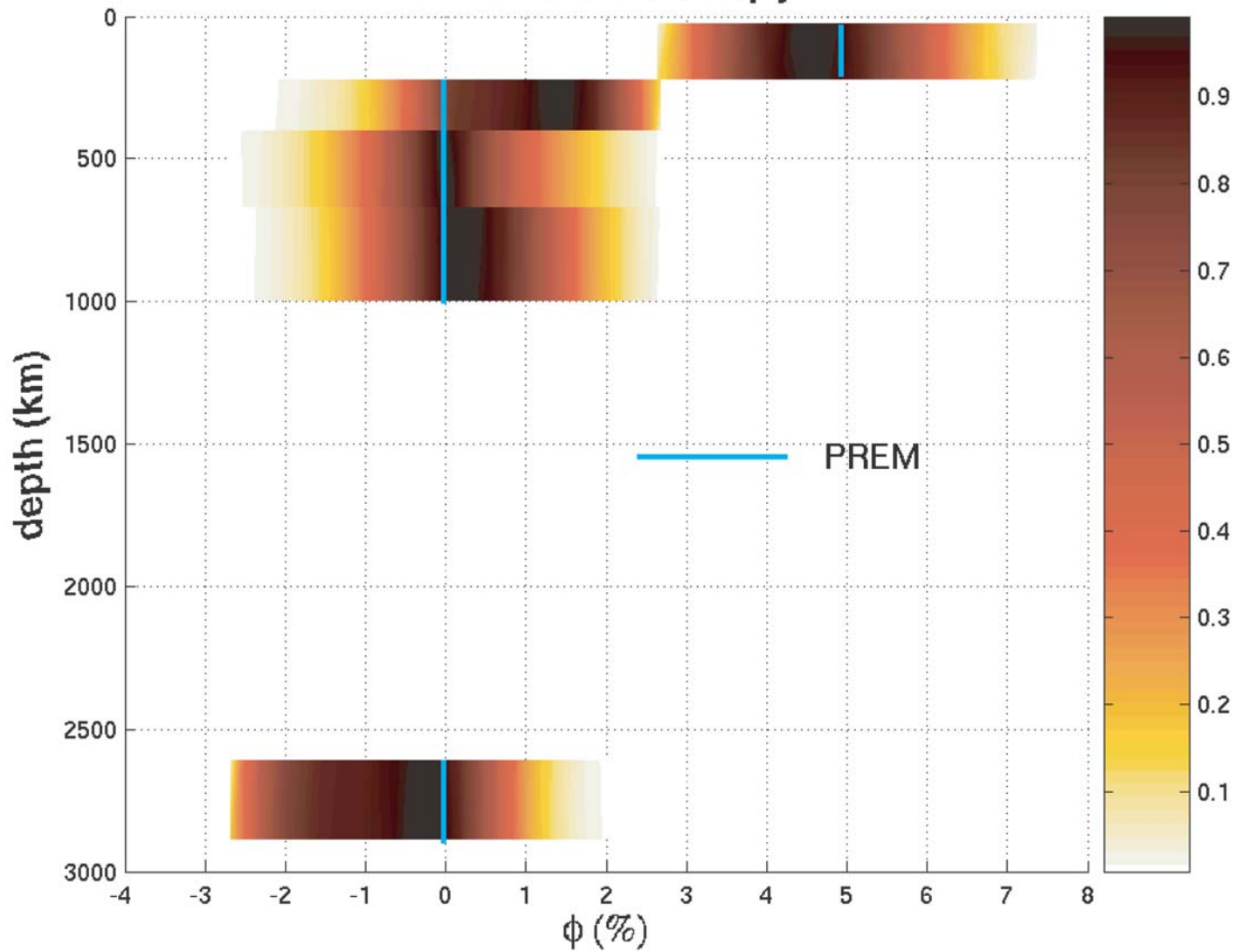
$\log(\text{period}(\text{s}))$

$\log(\text{period}(\text{s}))$

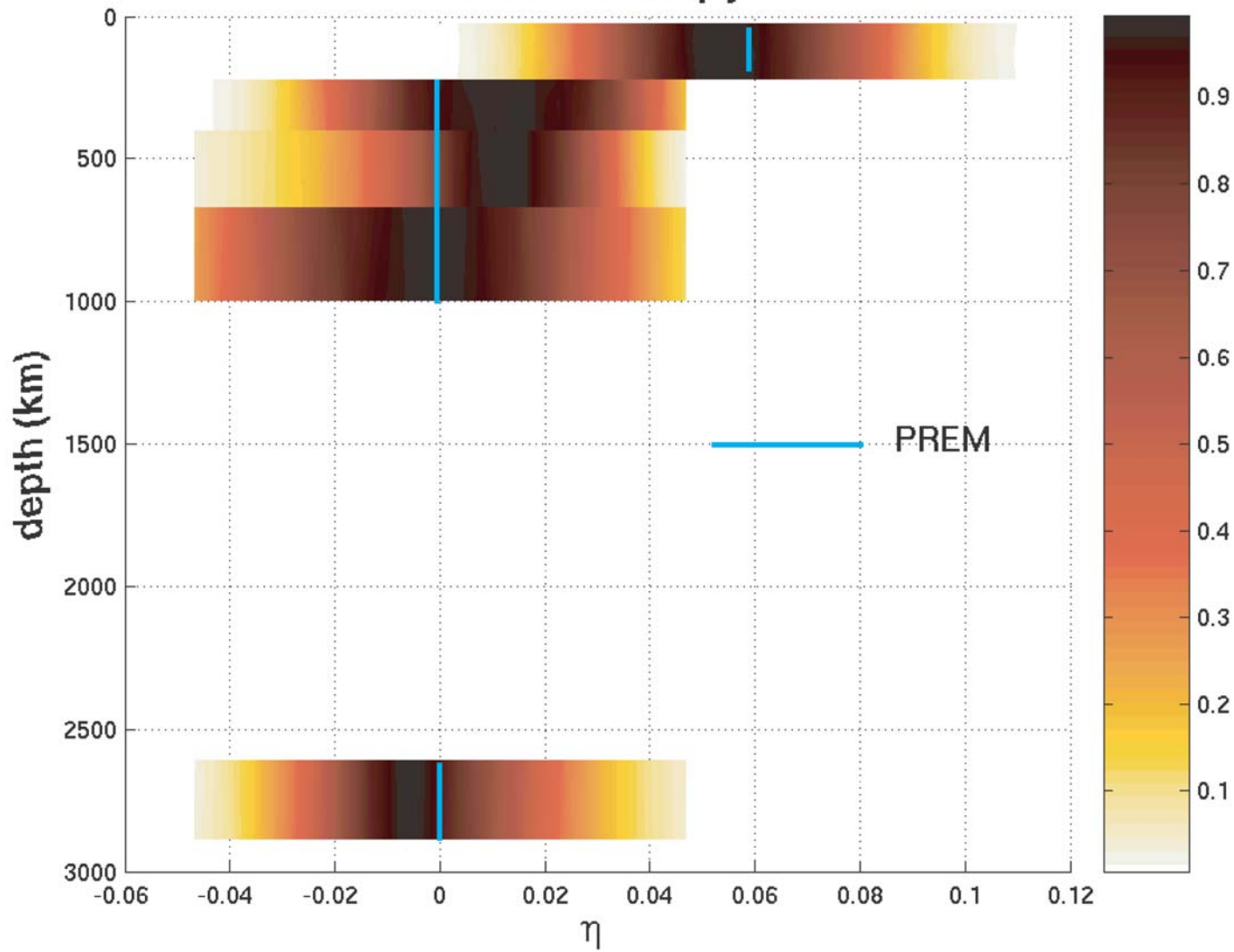
# Shear-wave anisotropy



# P-wave anisotropy



# Eta anisotropy



# Relative density anomalies

